

The presence and role of the intermediary CO reservoir in heterogeneous electroreduction of CO₂

Authors: Sheena Louisia^{1,2,5}, Dohyung Kim^{1,2,3,5}, Yifan Li^{1,2}, Mengyu Gao³, Sunmoon Yu^{2,3}, and Peidong Yang^{1,2,3,4}

Affiliations:

¹Department of Chemistry, University of California, Berkeley, CA, USA.

²Chemical Sciences Division, Lawrence Berkeley National Laboratory, Berkeley, CA, USA.

³Department of Materials Science and Engineering, University of California, Berkeley, CA, USA.

⁴Kavli Energy NanoScience Institute, Berkeley, CA, USA.

⁵These authors contributed equally to this work.

*Correspondence to: p_yang@berkeley.edu

Abstract

Despite the importance of the microenvironment in heterogeneous electrocatalysis, its role remains unclear due to a lack of suitable characterization techniques. Multi-step reactions like the electroconversion of CO_2 to multicarbonyls (C_{2+}) are especially relevant considering the potential creation of a unique microenvironment as part of the reaction pathway. To elucidate the significance of the microenvironment during CO_2 reduction, we develop on-stream substitution of reactant isotope (OSRI), a new method which relies on the subsequent introduction of CO_2 isotopes. Combining electrolytic experiments with a numerical model, this method reveals the presence of a reservoir of CO molecules concentrated near the catalyst surface that influences C_{2+} formation. Application of OSRI on a Cu nanoparticle (NP) ensemble and an electropolished Cu foil demonstrates that a CO monolayer covering the surface does not provide the amount of CO intermediates necessary to facilitate C-C coupling. Specifically, the C_{2+} turnover increases only after reaching a density of ~ 100 CO molecules per surface Cu atom. The Cu NP ensemble satisfies this criterion at an overpotential 100 mV lower than the foil, making it a better candidate for efficient C_{2+} formation. Furthermore, given the same reservoir size, the ensemble's intrinsically higher C-C coupling ability is highlighted by the 4-fold higher C_{2+} turnover it achieves at a more positive potential. The OSRI method provides an improved understanding of how the presence of CO intermediates in the microenvironment impacts C_{2+} formation during the electroreduction of CO_2 on Cu surfaces.

Introduction

Powering the conversion of small molecules into value-added products using renewable electricity is a promising approach to achieve sustainable production of fuels and chemicals.¹⁻³ The field of electrocatalysis has been moving towards this goal but remains hampered by activity and selectivity challenges. A molecular-level understanding of reactions is required to overcome these difficulties. More importantly, it should involve a thorough consideration of all factors that influence electrochemical conversion at heterogeneous surfaces. Previous studies have suggested that environmental aspects beyond the surface active site may be as critical for facilitating electrocatalytic reactions.^{4,5}

Studies in heterogeneous electrocatalysis have largely focused on controlling the active sites and understanding how it influences reaction pathways through techniques such as surface spectroscopy (e.g., *in situ* Raman and IR spectroscopy) combined with theory.⁶⁻⁸ However, locally confined environments also play a critical role in mediating reactions as demonstrated in other fields of catalysis. For example, in biocatalysis and homogeneous catalysis, the role of the microenvironment and the secondary coordination sphere have been widely investigated, respectively.⁹⁻¹⁴ The high selectivity achieved by bio- and molecular catalysts has often been associated with the characteristics of such regimes. Likewise, understanding the influence of a microenvironment in the context of heterogeneous electrocatalysis is necessary to gain better control of reactions. It is expected that the microenvironment created near a catalytically active surface will exhibit specific physicochemical properties that differ from the bulk.

Microenvironment effects may be especially important for the CO₂ reduction reaction (CO₂RR), particularly on Cu catalysts where a variety of value-added, higher-order products (e.g., ethylene, ethanol) are generated.¹⁵ Up to now, probing key surface intermediates using surface

spectroscopy coupled with theoretical calculations has led to the consensus that *CO is necessary for the formation of multicarbons (C₂₊).¹⁶⁻¹⁸ Further investigation has revealed the importance of its binding mode (i.e., *CO_{atop} or *CO_{bridge}) in determining CO₂RR selectivity.¹⁹⁻²¹ Other studies have reported high *CO coverage leading to C-C coupling necessary for C₂₊ formation.^{22,23} However, beyond the surface bound *CO, recent findings suggest the presence of near-surface CO species during CO₂ electroreduction relevant to C₂₊ formation.²⁴⁻²⁷ Furthermore, structural modifications presumed to affect the environment surrounding catalysts have been shown to improve C₂₊ selectivity.^{20,28-30} Considering its critical influence, an in-depth characterization of the microenvironment under CO₂ electroreduction conditions is needed.

However, the characteristics of the microenvironment remain elusive due to the lack of suitable techniques. Despite the insights acquired into surface species present during the reaction, the use of surface spectroscopy has been limited to analytes present within a few nanometers from the surface.^{31,32} Vibrational spectroscopy methods, such as Raman or FTIR, are also constrained to rely on surface enhancing effects to overcome the signal loss associated with the electrolyte.^{33,34} Additionally, the enhancement decays rapidly away from the surface (inversely proportional to the cube of the distance), exclusively favoring surface bound species.³⁵⁻³⁷ At high catalytic rates, optical interference from product bubble formation limits the use of such techniques under catalytically relevant *operando* conditions.^{26,38} Overall, the limitations of surface vibrational spectroscopy prevent it from understanding the microenvironment during electrochemical reactions on heterogeneous surfaces.

In this work, we present on-stream substitution of reactant isotope (OSRI) as a new method that can provide insights into the microenvironment near Cu surfaces during CO₂RR. The OSRI method employs isotopic labeling of the reagent CO₂ in a specific sequence and monitors its

transformation to various products. Through the analysis of product isotopic compositions, it reveals the presence of a reservoir of intermediary CO (CO_{int}) molecules necessary for C_{2+} formation. Applied to two different systems (i.e., Cu nanoparticle (NP) ensemble and polycrystalline Cu foil), a density reaching ~ 100 CO_{int} molecules per surface Cu atom is identified as a common characteristic of the reservoir linked to CO_2 conversion to multicarbons. Furthermore, the intrinsic C-C coupling ability of a catalyst can be gauged independently from the availability of CO_{int} . Ultimately, we find that the higher C_{2+} turnover of the Cu nanoparticles compared against the Cu foil originates from both its ability to form a large CO_{int} reservoir at low overpotentials and its intrinsically higher C-C coupling rate. Through the OSRI method, we identify the importance of a CO_{int} reservoir in the formation of C_{2+} over Cu surfaces, which has remained inaccessible thus far from conventional spectroscopic techniques.

Results

The OSRI method starts with the application of a cathodic bias under $^{12}\text{CO}_{2(\text{g})}$ at a constant flow in aqueous conditions for one hour, followed by a consecutive hour in which $^{12}\text{CO}_{2(\text{g})}$ feed is substituted with $^{13}\text{CO}_{2(\text{g})}$ under continued bias (Fig. 1a). The propagation of ^{13}C can then be tracked across all products generated during electrolysis, using multiple modes of product analysis in both the gas and liquid phase that quantify the isotopic compositions of different products (Fig. 1b). Throughout the two hours, the outlet gas stream is sampled at regular intervals by gas chromatography (GC) for product quantification in real-time. Furthermore, since the products contain a mix of ^{12}C and ^{13}C after switching to $^{13}\text{CO}_{2(\text{g})}$, the gas products during the second hour are collected in a gas bag (gas bag #1) to study their isotopic composition by gas chromatography-mass spectrometry (GC-MS) (Supplementary Fig. 1 and Text 1). Finally, the liquid products accumulated in the catholyte, as well as the membrane during OSRI, are analyzed using ^1H and ^{13}C NMR (Supplementary Texts 2-3). Consequently, both the production rate and the isotopic composition of all formed products can be determined (Methods). Throughout OSRI, the current density and product faradaic efficiencies remained stable (Supplementary Fig. 9). All potentials are reported on the reversible hydrogen electrode (RHE) scale.

The first catalytic system studied by OSRI was an ensemble of 7 nm Cu nanoparticles (NPs) as reported in previous studies at -0.60 V with CO and HCOO^- as CO_2RR products.³⁹ Because the complete exchange of ^{13}C for the $^{12}\text{CO}_{2(\text{aq})}$ is delayed by its equilibration with $\text{H}^{12}\text{CO}_3^-$ (aq), the overall average of $^{12}\text{CO}_{2(\text{aq})}$ available should be $> 50\%$ (Fig. 1a). As expected, while the $^{12}\text{C}:^{13}\text{C}$ ratio of $\text{CO}_{2(\text{g})}$ supplied was 1:1, all products were found with a consistently higher ^{12}C content (Fig. 2a). The delay of $\text{CO}_{2(\text{aq})}$ to complete the exchange was theoretically verified through a multiphysics simulation (Methods). Regardless of any $\text{CO}_{2(\text{aq})}$ consumption taking place at the

electrode due to applied potentials, there remains a substantial amount of $^{12}\text{CO}_{2(\text{aq})}$ available in solution after an hour of purging $^{13}\text{CO}_{2(\text{g})}$ into a $^{12}\text{CO}_{2(\text{g})}$ saturated 0.1M $\text{KH}^{12}\text{CO}_3$ electrolyte (Supplementary Fig. 10). The multiple equilibria following $\text{CO}_{2(\text{g})}$ dissolution including $\text{HCO}_3^-(\text{aq})$ and $\text{CO}_3^{2-}(\text{aq})$ are responsible for the slow exchange of all ^{12}C in solution (Supplementary Text 4 and Supplementary Fig. 11). It should be noted that the colored segments for $\text{CO}_{2(\text{aq})}$ and the products in Fig. 1a are simply divided to qualitatively depict their average composition during OSRI; however, the true isotopic shift from ^{12}C to ^{13}C takes place gradually throughout the two hours as shown in Supplementary Figures 10 and 11. Varying the flow rate of $\text{CO}_{2(\text{g})}$ or the rate of $\text{CO}_{2(\text{aq})}$ consumption results in changes in the isotopic composition of electrolytically available $\text{CO}_{2(\text{aq})}$ that are consistent with this analysis (Supplementary Text 5 and Supplementary Fig. 12).

Although both CO and HCOO^- are enriched in ^{12}C due to the electrolyte equilibration, CO is more enriched in ^{12}C than HCOO^- (Fig. 2a). The difference in isotopic composition likely originates from the CO_2 -to- HCOO^- mechanism which, unlike CO_2 -to-CO conversion, is known for not involving CO as an intermediate (e.g., $^*\text{CO}$).⁴⁰⁻⁴² Without an accumulation of intermediates involved in HCOO^- formation, its isotopic composition should closely track that of $\text{CO}_{2(\text{aq})}$ *available* during OSRI. On the other hand, a buildup of CO population on a Cu surface is expected for CO formation.^{40,43,44} In previous works, this buildup of CO has been suggested to result in a locally concentrated near-surface CO acting as an intermediate state for CO, and eventually, other higher-order product formation (e.g., C_2H_4).^{24,25,27} This hypothesis has inspired improved CO_2 reduction strategies by combining CO generating catalysts (e.g., Ag, Au) with Cu-based electrodes.⁴⁵⁻⁴⁸ Furthermore, these studies infer that chemically adsorbed CO (i.e., $^*\text{CO}$) may not be the only configuration of CO as an intermediate. Therefore, we refer to all CO species during CO_2 electroreduction, whether chemically bound or otherwise physically confined near the catalyst

surface, as CO_{int} . The buildup and formation of a large reservoir of CO_{int} will lead to a lag between the available $\text{CO}_{2(\text{aq})}$ (reagent) and CO (product) released at steady-state. Specifically, in an experiment that switches from one isotope of $\text{CO}_{2(\text{aq})}$ (^{12}C) to another (^{13}C), CO produced is expected to be more enriched in ^{12}C than the average isotopic composition of available $\text{CO}_{2(\text{aq})}$ (Fig. 1a).

To understand this isotopic lag phenomenon quantitatively, we construct a mathematical model that describes a CO_{int} reservoir attached to a Cu surface during OSRI (Fig. 2b). The applicability of the model to the experimental observations was evaluated and confirmed based on its close reproduction of four key experimental results: ① the average isotopic fraction of $\text{H}^{12}\text{COO}^-$, ② the average isotopic fraction of ^{12}CO , ③ the density of the CO_{int} reservoir per surface Cu atom (Cu_{surf}), and ④ the isotopic fraction of $^{12}\text{CO}_{\text{int}}$ at the CO_{int} reservoir by the end of OSRI (details available in Supplementary Text 6). Owing to the presence of the CO_{int} reservoir, the model reproduced the delayed exchange to ^{13}C in the CO produced, leading to the trends shown in Figure 2b for the isotopic fraction of $\text{H}^{12}\text{COO}^-$ and ^{12}CO over time. Values ① and ② are essentially the areas of each curve for $\text{H}^{12}\text{COO}^-$ and ^{12}CO divided by the entire period (i.e., 120 min), respectively. Furthermore, the steady state ③ size of the CO_{int} reservoir predicted by the model can be compared to the experimental value measured after stopping the bias at the end of the second hour of OSRI. All CO present in the cell then is purged with Ar for one hour and collected in gas bag #2 (Fig. 1c). The amount of CO_{int} present at steady state near the Cu surface is determined after quantifying all the collected CO and subtracting the headspace and bulk electrolyte dissolved CO contributions (Methods and Supplementary Fig. 15). The number of Cu_{surf} necessary to determine the CO_{int} density per Cu_{surf} atom can be derived from Pb underpotential deposition (Methods and Supplementary Text 7). The model also predicts the trend of the isotopic fraction of $^{12}\text{CO}_{\text{int}}$

throughout OSRI leading to value ④ at 120 min (Supplementary Fig. 13d). The model-derived isotopic fraction of $^{12}\text{CO}_{\text{int}}$ at this final time point can be compared to the experimental isotopic fraction, measured as 54% ^{12}CO , for all CO remaining post-electrolysis and collected in gas bag #2 (Fig. 1c). Overall, the model closely reproduced the experimental values as summarized in Fig. 2c.

As stated earlier, the difference in isotopic composition between values ① and ② is a result of the CO_{int} reservoir being present during CO_2 electrolysis. Changing experimental conditions to accelerate the rate of $\text{CO}_{2(\text{aq})}$ exchange from ^{12}C to ^{13}C (e.g., by the use of a liquid flow cell simultaneously switching to a $\text{KH}^{13}\text{CO}_3$ electrolyte) does not alter this difference (Supplementary Fig. 17). The duration of operation upon substituting to $^{13}\text{CO}_{2(\text{g})}$ is another parameter that could be considered, and a longer electrolysis period is not desirable as the larger amount of total products formed obscures the relative difference between $\text{H}^{12}\text{COO}^-$ and ^{12}CO (Supplementary Fig. 18). Altogether, the chosen experimental conditions that define OSRI are adequate to assess the presence of the CO_{int} reservoir.

The results obtained from OSRI and reproduced by the model confirm the hypothesis of a CO_{int} reservoir present during CO_2RR . Furthermore, the size of the CO_{int} reservoir verified offers new insights into the local environment of catalytically active Cu surfaces during CO_2 electrolysis. We find that the CO_{int} density is around 78 CO_{int} per Cu_{surf} , which is much higher than monolayer coverage expected for $^*\text{CO}$ alone (i.e., 1 CO_{int} per Cu_{surf}) (Fig. 2b). Assuming that this density of CO_{int} molecules is confined in a volume extending as far as $\sim 100\ \mu\text{m}$ from the electrode (i.e., up to the Nernst diffusion layer), then its concentration is approximately 18 mM (where typical CO solubility in water is 1 mM). Such a supersaturation condition (20 to 100 times the solubility) has been considered near the surface of gas evolving electrodes and is often associated with gas bubble

nucleation and growth.⁴⁹⁻⁵¹ Considering the physical properties of CO and theoretical aspects of supersaturation, CO is expected to exist in a supersaturated state on a CO-producing electrode that may be even > 18 mM (Supplementary Text 8). Therefore, we expect the physical state of CO_{int} to exist somewhere between a supersaturated dissolved state and a gas phase.

To understand the role of the CO_{int} reservoir in the formation of C_{2+} products, we investigated more negative potentials where CO_2 -to- C_{2+} conversion takes place. Experimentally, not only were the C_{2+} products also higher in ^{12}C content relative to HCOO^- , but they shared a similar average isotopic composition with CO, highly suggesting that the CO_{int} reservoir acts both as a source of product CO and as an intermediate pool for C_{2+} (Supplementary Fig. 19). The model was therefore expanded to reproduce the isotopic composition of C_{2+} products, as well as HCOO^- and CO, at more negative potentials. The conversion rate of the CO_{int} reservoir was adjusted to include the amount of CO_{int} consumed to C_{2+} products (Supplementary Text 9). Once more, the model was found to closely reproduce the experimental data obtained during OSRI supporting the CO_{int} reservoir as an intermediate to C_{2+} formation. For instance, the isotopic composition of gas products measured in real time by GC-MS for the CO-derived products, such as CO and C_2H_4 , matched closely with the trend expected by the model (Fig. 3a and Supplementary Fig. 21). Furthermore, the model closely replicated all the experimental values ①-④ (Supplementary Fig. 20). Overall, instead of the traditional reaction pathway of CO_2 to surface-bound $^*\text{CO}$ and then to C_{2+} products, we posit that CO_2 first reduces to CO_{int} which accumulates to a concentrated reservoir near the catalyst surface before subsequent conversion to higher-order products (Fig. 3b).

Additionally, only a small fraction of the CO_{int} reservoir is converted per second to produce CO, C_2H_4 , EtOH, and n-PrOH (Fig. 3c). The relative portion of the CO_{int} reservoir utilized per unit time ($\% \text{ s}^{-1}$) does not increase significantly and reaches only up to 1.05% per second as the potential

is biased more negative. Instead, the distribution of products formed from the CO_{int} reservoir changes in favor of C_{2+} (Fig. 3d). Simultaneously, this shift in selectivity coincides with an increase of the CO_{int} density, roughly doubling from 78 to 147 molecules per Cu_{surf} (Fig. 3d). These observations suggest that C_{2+} -formation correlates with a sizeable amount of CO_{int} per Cu_{surf} ($\sim 100 \text{ CO}_{\text{int}}/\text{Cu}_{\text{surf}}$). Interestingly, we note that a CO_{int} reservoir conversion of 1.05% per sec is equivalent to a conversion rate of $\sim 1 \text{ CO}_{\text{int}}$ monolayer per sec. This indicates that, unlike a monolayer of CO_{int} , a large CO_{int} reservoir can sustain the necessary conditions to attain a conversion rate at the scale of a monolayer of intermediates per sec.

Previous works have commented on the importance of obtaining high CO surface coverage to facilitate C-C coupling.^{22,25,52} The OSRI results suggest that this configuration extends to a CO_{int} reservoir present near the catalyst surface which may act as the source for C_{2+} formation downstream. Hence, the former notion of the traditional $\ast\text{CO}$ monolayer is replaced with a locally concentrated large population of CO molecules as intermediates. Furthermore, OSRI experimentally verifies the often-speculated idea of CO-rich environments on the surface of CO_2 reduction catalysts.²⁴⁻²⁷

To verify that the CO_{int} reservoir is not unique to the Cu NP ensemble catalyst, the OSRI method was applied to an electropolished Cu foil, a well-known benchmark Cu catalyst for CO_2RR . The potential range selected to study the Cu foil was negatively shifted in comparison to the Cu NP ensemble to generate a similar product distribution (Supplementary Table 8 and Supplementary Fig. 22). Cu foil exhibits a similar gap in ^{12}C isotopic fraction between HCOO^- and all CO_{int} -derived products (Supplementary Fig. 23). However, a collection of gases (i.e., CO, CH_4 , and C_2H_4) was detected when trying to identify the contents of the reservoir experimentally as described in Fig. 1c (Supplementary Text 10). The presence of products such as CH_4 , together

with CO concentrated near the surface is expected to result from the morphological features of the Cu surface promoting retention of gases.⁵³ Therefore, the model was used to fit the Cu foil data while taking into consideration the presence of gases beyond CO as part of a larger reservoir regulating product formation and release (Supplementary Text 11). Ultimately, the model closely replicates the experimental data thus confirming the existence of a CO_{int} reservoir on Cu foil during CO₂RR (Supplementary Fig. 26).

Interestingly, both catalysts appear to enable C-C coupling after reaching a sufficiently high density of CO_{int} per Cu_{surf}. Similar to the Cu NP ensemble, analysis of the Cu foil indicates a transition from C₁ to C₂₊ formation at a CO_{int} density ranging between 100-150 CO_{int} per Cu_{surf} (Fig. 4a). The Cu foil further resembles the Cu NP ensemble with a CO_{int}-to-C₂₊ conversion rate of ~1 CO_{int} monolayer per sec which is achieved after reaching ~100 CO_{int} per Cu_{surf} (Supplementary Fig. 27). These results suggest that a high surface coverage restricted to a monolayer does not provide the amount of CO_{int} necessary for C₂₊ formation. Taken these data, a key consideration in the development of catalysts moving forward should be increasing the CO_{int} density at lower overpotentials. Accordingly, the Cu NP ensemble reaches an adequate CO_{int} density at an overpotential 100 mV lower than the foil (Fig. 4b).

In addition to producing a sufficiently dense CO_{int} reservoir, a catalyst's activity should also be determined by its innate ability to convert the CO_{int} reservoir to C₂₊. So far, Cu-based electrocatalysts have been evaluated based on their C₂₊ faradaic efficiency and turnover at a fixed potential. However, such analysis does not account for the availability of CO_{int}, which is critical; without the sufficient formation of CO_{int}, a catalyst is unlikely to form C₂₊ efficiently. Therefore, considering both the applied potential and availability of CO_{int} is necessary to accurately assess a catalyst's C-C coupling (i.e., the intrinsic C₂₊ formation from C₁ intermediates) ability. This is

readily apparent in the comparison of C_{2+} turnover between the Cu NP ensemble and the foil around -0.85 V where the former displays a CO_{int} reservoir nearly twice as large as the latter (Fig. 4b).

This difference in the size of the CO_{int} reservoir brings into question whether the Cu foil may yield a C_{2+} turnover comparable to the NP ensemble provided there is enough CO_{int} allowed at a lower overpotential. However, we find this unlikely given the trend in the C_{2+} TOF of the Cu foil (Fig. 4b). Despite reaching a CO_{int} density of ~ 100 CO_{int} per Cu_{surf} , its TOF does not rise steeply to reach comparable levels as the NP ensemble; a TOF of 0.1 C_{2+} per Cu_{surf} s^{-1} at -0.92 V is 4-fold lower than the NP ensemble whose TOF is 0.4 C_{2+} per Cu_{surf} s^{-1} at only -0.86 V. Furthermore, under CO reduction (CORR) conditions with identical CO availability, we find the NP ensemble to exhibit higher $TOF_{C_{2+}}$ than the Cu foil as well (Supplementary Fig. 28). Hence, the formation of a concentrated CO_{int} reservoir is necessary but not sufficient for high C_{2+} turnover.

In addition, both catalysts reach noticeably higher levels of $TOF_{C_{2+}}$ during CO_2RR in comparison to CORR (Supplementary Fig. 28). This likely results from the formation of the reservoir during the electroreduction of CO_2 , which sustains ~ 100 CO molecules per Cu_{surf} . In contrast, within the 100 μm layer away from the catalyst surface, only 5 CO molecules per Cu_{surf} would be available under CORR. The concentrated CO microenvironment formed during CO_2RR overcomes the constraint of low CO solubility (1mM in water at 1atm, room temperature) which limits CORR activity in aqueous conditions. Therefore, instead of the concentration of CO_2 , the size of the CO_{int} reservoir is a more accurate representation of the reactants necessary to the formation of multicarbons. We suggest that such considerations are also important for CO_2 reduction in gas-diffusion electrode (GDE) systems; recent works have reported the importance of optimizing both the CO_2 and CO availability to maximize C-C coupling.^{52,54,55}

The results from the OSRI method suggest that both the contribution of CO_{int} availability and intrinsic C-C coupling ability are necessary to a catalyst's CO₂-to-C₂₊ activity. Concretely, a good catalyst must possess the ability to form a large CO_{int} reservoir at low overpotentials as well as exhibit high intrinsic activity for the coupling of CO_{int}. The Cu foil's moderate C₂₊ intrinsic activity is ascribed not only to its low intrinsic C-C coupling capacity but also to the high overpotential required to form a large enough CO_{int} reservoir. Therefore, maximizing CO_{int} availability at low overpotentials emerges as an additional parameter in future catalyst design, in addition to the necessary structural traits that favor C-C coupling.^{39,56,57} Namely, CO_{int} availability can be enhanced through improved retention of CO upon its formation. A few approaches along this line have been considered, such as modifying surface morphologies of electrodes to impact product release or functionalizing the catalyst with surface additives that promote gas affinity through increased hydrophobicity.^{28,58-60} Beyond catalyst design implications, these results indicate that further investigations to determine the intrinsic C-C coupling of Cu-based catalysts under controlled (micro)environments are needed.

In summary, we present OSRI, a unique method that probes the microenvironment surrounding Cu surfaces during CO₂RR. It has led to the discovery of a concentrated reservoir of CO molecules near catalyst surfaces which is necessary for efficient C-C coupling. Instead of CO₂, this reservoir is identified as a more accurate representation of the reactants determining the rate of multicarbon formation during CO₂RR. Through these findings, the importance of the microenvironment formed during the reaction is better distinguished from the intrinsic activity of the catalyst surface. Furthermore, OSRI is a promising method to investigate the effects of the microenvironment in other catalytic reactions similar to CO₂RR. Specifically, the significance of

intermediates residing near the surface during multi-step electrocatalytic reactions can be gauged, thus guiding future improvements in catalysts' selectivity and activity.

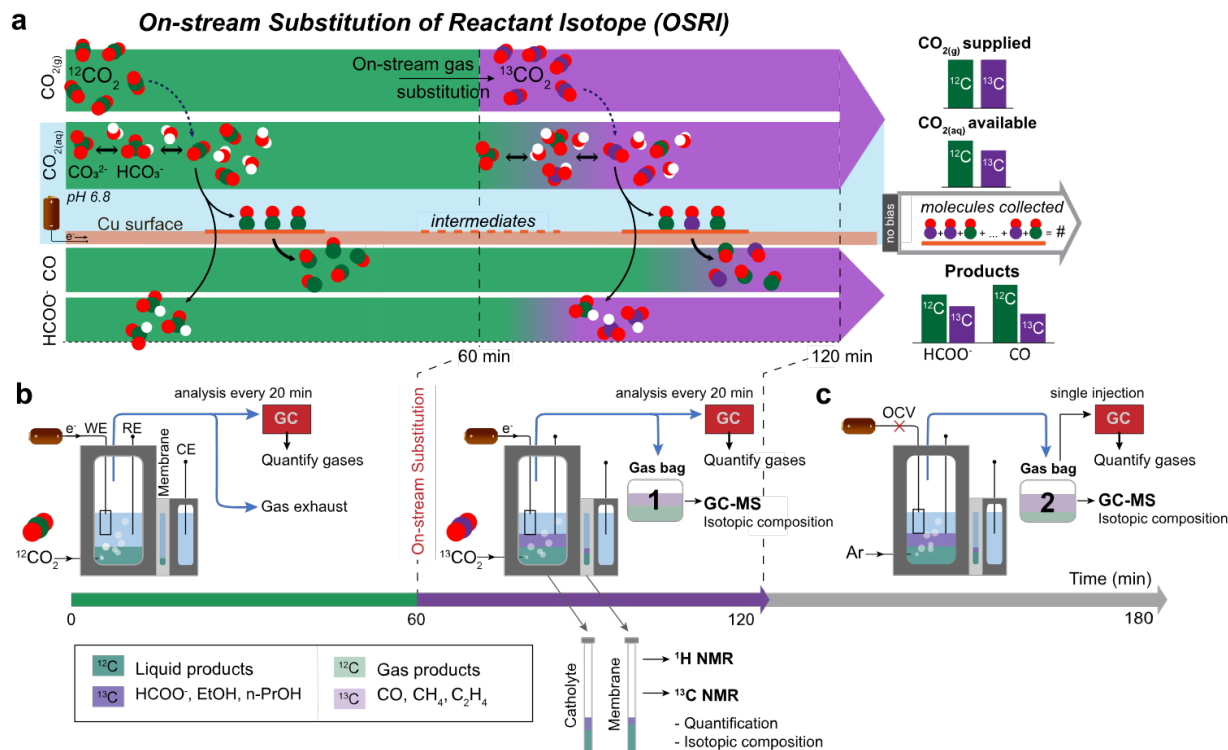


Figure 1. Study of Cu for CO₂ electroreduction by OSRI. **a**, Schematic describing OSRI and the catalytic results of Cu. Cathodic bias is applied and maintained for 2 hours while the 0.1 M KH¹²CO₃ electrolyte is purged with ¹²CO_{2(g)} (green) for the first hour followed by ¹³CO_{2(g)} (purple) during the second hour. **b**, The experimental setup of OSRI. Products that contain ¹²C (green) and ¹³C (purple) accumulate in the gas (gas bag #1) and liquid phase (electrolyte) for isotopic analysis by GC-MS and NMR, respectively. All effluent gases are collected in gas bag #1 for the second hour only. Regular quantification of gas products is conducted by sampling the outlet stream at 20 minute intervals by GC. NMR spectroscopy is used to quantify and determine the isotopic composition of the liquid products accumulated after 2 hours in both the catholyte and the anionic membrane. Formate is the only product that accumulates in the membrane during OSRI. **c**, After 2 hours of electrolysis, the application of bias is terminated, and the electrolyte is purged with Ar into a second gas bag (gas bag #2) for another hour to collect all the gases remaining in the chamber.

The contents of gas bag #2 are analyzed using GC (quantification) and GC-MS (isotopic composition).

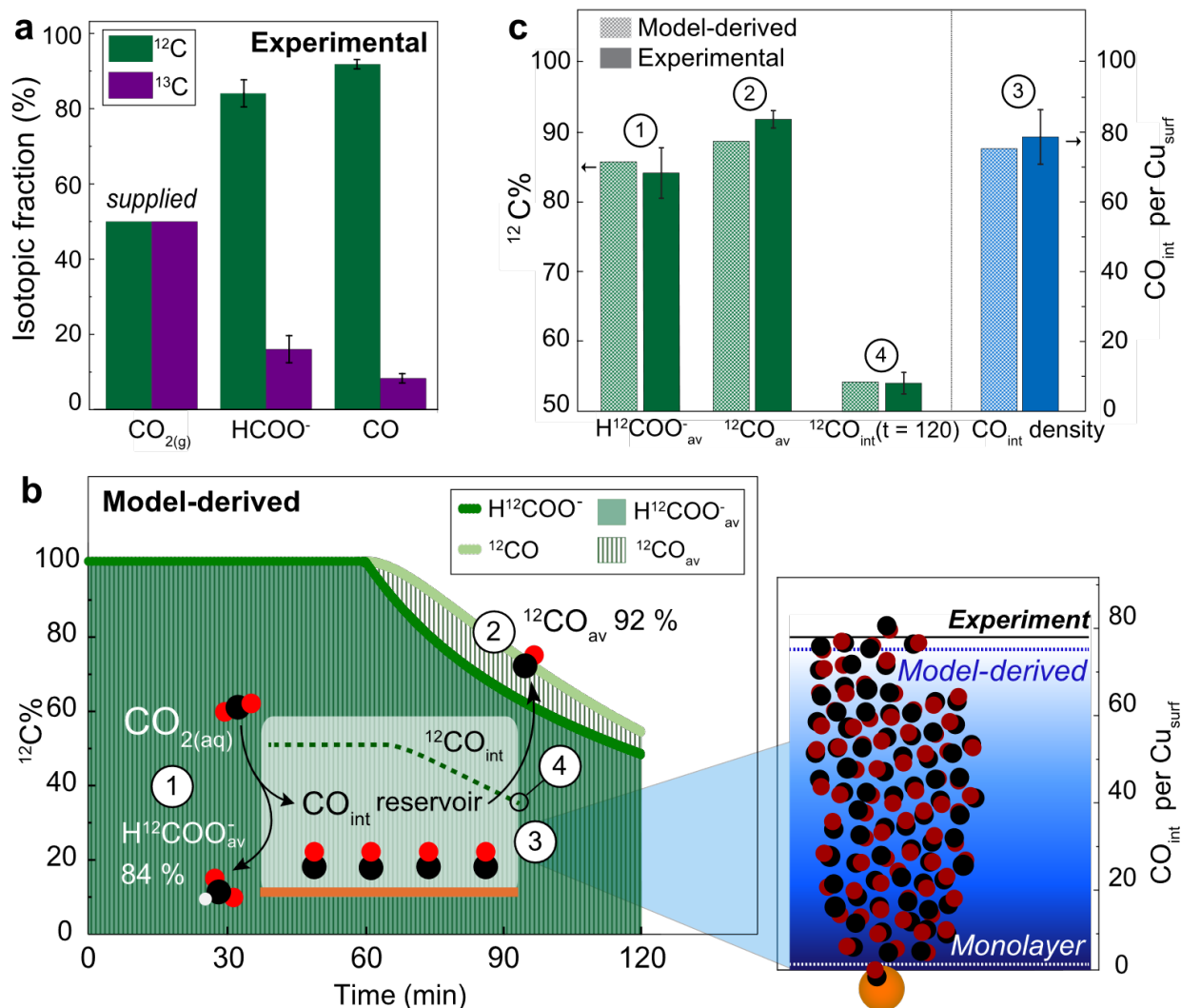


Figure 2. Identification of the CO_{int} reservoir on the Cu NP ensemble. **a**, Isotopic composition of $\text{CO}_{2(\text{g})}$ supplied and the products of CO_2RR measured during OSRI at -0.6 V vs RHE. **b**, Model-derived ^{12}C content of CO and HCOO^- produced overtime during OSRI considering the presence of a CO_{int} reservoir of constant size at steady state. The areas under each curve divided by the total period (2 hrs) indicate the average isotopic fraction of ① $^{12}\text{HCOO}^-$ and ② ^{12}CO for the entire run. ④ $^{12}\text{CO}_{\text{int}}$ at the end of OSRI correspond to $^{12}\text{CO}_{\text{int}}(t = 120 \text{ min})$. The ③ steady state density of CO_{int} per Cu_{surf} measured experimentally and reproduced by the model are illustrated and compared to the monolayer of adsorbed $^*\text{CO}$. The number of Cu_{surf} was estimated by measuring

the electrochemically active surface area by Pb underpotential deposition. **c**, Comparison of model-derived and experimental values for the average isotopic fraction of ① $\text{H}^{12}\text{COO}^-$ and ② ^{12}CO during OSRI, ③ the steady state CO_{int} density, and ④ the isotopic fraction $^{12}\text{CO}_{\text{int}}(t = 120 \text{ min})$. Error bars are one standard deviation of three independent measurements for the experimental data.

The number of CO_{int} converted to each product is labeled as $n \times \text{CO}_{\text{int}}$, where n corresponds to the number of CO_{int} required for its formation (e.g., $2 \times \text{CO}_{\text{int}}$ for C₂H₄). Error bars are one standard deviation of three independent measurements.

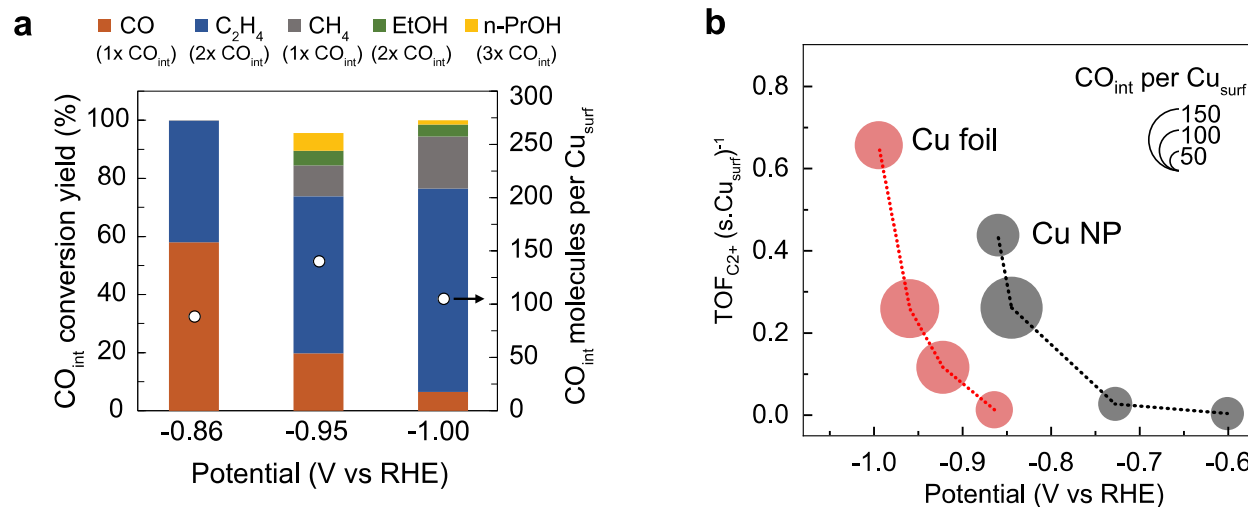


Figure 4. Comparison between the Cu foil and the Cu NP ensemble. **a**, CO_{int} conversion yield (CO_{int} consumed for each product/all CO_{int} consumed) partitioned across different CO_{int}-derived products and CO_{int} density measured as a function of applied potential on the Cu foil. The number of CO_{int} converted to each product is labeled as $n \times \text{CO}_{\text{int}}$, where n corresponds to the number of CO_{int} required for its formation (e.g., $2 \times \text{CO}_{\text{int}}$ for C₂H₄). **b**, C₂⁺ turnover (dashed line) of the Cu foil and Cu NP ensemble with their CO_{int} density (by the size of the bubble) as a function of applied potential. Bubbles are plotted to scale with respect to their diameter.

References

- 1 De Luna, P. *et al.* What would it take for renewably powered electrosynthesis to displace petrochemical processes? *Science* **364** (2019).
- 2 Blanco, D. E. & Modestino, M. A. Organic electrosynthesis for sustainable chemical manufacturing. *Trends in Chemistry* **1**, 8-10 (2019).
- 3 Na, J. *et al.* General technoeconomic analysis for electrochemical coproduction coupling carbon dioxide reduction with organic oxidation. *Nat. Comm.* **10**, 1-13 (2019).
- 4 Kim, D. *et al.* Selective CO₂ electrocatalysis at the pseudocapacitive nanoparticle/ordered-ligand interlayer. *Nat. Energy*, 1-11 (2020).
- 5 Ramaswamy, N. *et al.* Hydrogen oxidation reaction in alkaline media: Relationship between electrocatalysis and electrochemical double-layer structure. *Nano Energy* **41**, 765-771 (2017).
- 6 Chen, W. *et al.* Probing complex electrocatalytic reactions using electrochemical infrared spectroscopy. *Curr. Opin. Electrochem.* **14**, 113-123 (2019).
- 7 Zaera, F. Probing liquid/solid interfaces at the molecular level. *Chem. Rev.* **112**, 2920-2986 (2012).
- 8 Zhu, Y., Wang, J., Chu, H., Chu, Y.-C. & Chen, H. M. In Situ/Operando Studies for Designing Next-Generation Electrocatalysts. *ACS Energy Lett.* **5**, 1281-1291 (2020).
- 9 Lancaster, L., Abdallah, W., Banta, S. & Wheeldon, I. Engineering enzyme microenvironments for enhanced biocatalysis. *Chem. Soc. Rev.* **47**, 5177-5186 (2018).
- 10 Colquhoun, H. M., Stoddart, J. F. & Williams, D. J. Second-Sphere Coordination—a Novel Role for Molecular Receptors. *Angew. Chem. Int. Ed. in English* **25**, 487-507 (1986).
- 11 Hale, L. V. & Szymczak, N. K. Hydrogen transfer catalysis beyond the primary coordination sphere. *ACS Catal.* **8**, 6446-6461 (2018).
- 12 Cao, Y., Li, X. & Ge, J. Enzyme Catalyst Engineering toward the Integration of Biocatalysis and Chemocatalysis. *Trends Biotechnol.* (2021).
- 13 Vázquez-González, M., Wang, C. & Willner, I. Biocatalytic cascades operating on macromolecular scaffolds and in confined environments. *Nat. Catal.* **3**, 256-273 (2020).
- 14 Zhang, Y., Wang, Q. & Hess, H. Increasing enzyme cascade throughput by pH-engineering the microenvironment of individual enzymes. *ACS Catal.* **7**, 2047-2051 (2017).
- 15 Nitopi, S. *et al.* Progress and perspectives of electrochemical CO₂ reduction on copper in aqueous electrolyte. *Chem. Rev.* **119**, 7610-7672 (2019).
- 16 Kim, Y. *et al.* Time-resolved observation of C–C coupling intermediates on Cu electrodes for selective electrochemical CO₂ reduction. *Energy Environ. Sci.* **13**, 4301-4311 (2020).
- 17 Pérez-Gallent, E., Figueiredo, M. C., Calle-Vallejo, F. & Koper, M. T. Spectroscopic observation of a hydrogenated CO dimer intermediate during CO reduction on Cu (100) electrodes. *Angew. Chem.* **129**, 3675-3678 (2017).
- 18 Wuttig, A., Ryu, J. & Surendranath, Y. Electrolyte competition controls surface binding of CO intermediates to CO₂ reduction catalysts. *Preprint at <https://doi.org/10.26434/chemrxiv>* **7929038**, v2 (2019).
- 19 Li, F. *et al.* Molecular tuning of CO 2-to-ethylene conversion. *Nature* **577**, 509-513 (2020).
- 20 Chou, T.-C. *et al.* Controlling the oxidation state of the Cu electrode and reaction intermediates for electrochemical CO₂ reduction to ethylene. *J. Am. Chem. Soc.* **142**, 2857-2867 (2020).
- 21 Gunathunge, C. M., Ovalle, V. J., Li, Y., Janik, M. J. & Waagele, M. M. Existence of an electrochemically inert CO population on Cu electrodes in alkaline pH. *ACS Catal.* **8**, 7507-7516 (2018).
- 22 Huang, Y., Handoko, A. D., Hirunsit, P. & Yeo, B. S. Electrochemical reduction of CO₂ using copper single-crystal surfaces: effects of CO* coverage on the selective formation of ethylene. *ACS Catal.* **7**, 1749-1756 (2017).
- 23 Sandberg, R. B., Montoya, J. H., Chan, K. & Nørskov, J. K. CO-CO coupling on Cu facets: Coverage, strain and field effects. *Surf. Sci.* **654**, 56-62 (2016).

- 24 Wuttig, A. *et al.* Tracking a common surface-bound intermediate during CO₂-to-fuels catalysis. *ACS Cent. Sci.* **2**, 522-528 (2016).
- 25 Clark, E. L. & Bell, A. T. Direct observation of the local reaction environment during the electrochemical reduction of CO₂. *J. Am. Chem. Soc.* **140**, 7012-7020 (2018).
- 26 Jiang, S., Klingan, K., Pasquini, C. & Dau, H. New aspects of operando Raman spectroscopy applied to electrochemical CO₂ reduction on Cu foams. *J. Chem. Phys.* **150**, 041718 (2019).
- 27 Klingan, K. *et al.* Reactivity determinants in electrodeposited Cu foams for electrochemical CO₂ reduction. *ChemSusChem* **11**, 3449-3459 (2018).
- 28 Wakerley, D. *et al.* Bio-inspired hydrophobicity promotes CO₂ reduction on a Cu surface. *Nat. Mater.* **18**, 1222-1227 (2019).
- 29 Baturina, O. *et al.* Effect of nanostructured carbon support on copper electrocatalytic activity toward CO₂ electroreduction to hydrocarbon fuels. *Catal. Today* **288**, 2-10 (2017).
- 30 O'Mara, P. B. *et al.* Cascade reactions in nanozymes: Spatially separated active sites inside Ag-Core-Porous-Cu-shell nanoparticles for multistep carbon dioxide reduction to higher organic molecules. *J. Am. Chem. Soc.* **141**, 14093-14097 (2019).
- 31 Dunwell, M. *et al.* Examination of near-electrode concentration gradients and kinetic impacts on the electrochemical reduction of CO₂ using surface-enhanced infrared spectroscopy. *ACS Catal.* **8**, 3999-4008 (2018).
- 32 Heyes, J., Dunwell, M. & Xu, B. CO₂ reduction on Cu at low overpotentials with surface-enhanced in situ spectroscopy. *J. Phys. Chem. C* **120**, 17334-17341 (2016).
- 33 Heidary, N., Ly, K. H. & Kornienko, N. Probing CO₂ conversion chemistry on nanostructured surfaces with Operando vibrational spectroscopy. *Nano Lett.* **19**, 4817-4826 (2019).
- 34 Handoko, A. D., Wei, F., Yeo, B. S. & Seh, Z. W. Understanding heterogeneous electrocatalytic carbon dioxide reduction through operando techniques. *Nat. Catal.* **1**, 922-934 (2018).
- 35 Osawa, M., Ataka, K.-I., Yoshii, K. & Nishikawa, Y. Surface-enhanced infrared spectroscopy: the origin of the absorption enhancement and band selection rule in the infrared spectra of molecules adsorbed on fine metal particles. *Appl. Spectrosc.* **47**, 1497-1502 (1993).
- 36 Schatz, G. C. Theoretical studies of surface enhanced Raman scattering. *Acc. Chem. Res.* **17**, 370-376 (1984).
- 37 Stiles, P. L., Dieringer, J. A., Shah, N. C. & Van Duyne, R. P. Surface-enhanced Raman spectroscopy. *Annu. Rev. Anal. Chem.* **1**, 601-626 (2008).
- 38 Kas, R. *et al.* In-situ infrared spectroscopy applied to the study of the electrocatalytic reduction of CO₂: Theory, practice and challenges. *ChemPhysChem* (2019).
- 39 Li, Y. *et al.* Electrochemically scrambled nanocrystals are catalytically active for CO₂-to-multicarbon. *Proc. Natl. Acad. Sci. USA* **117**, 9194-9201 (2020).
- 40 Peterson, A. A., Abild-Pedersen, F., Studt, F., Rossmeisl, J. & Nørskov, J. K. How copper catalyzes the electroreduction of carbon dioxide into hydrocarbon fuels. *Energy Environ. Sci.* **3**, 1311-1315 (2010).
- 41 Hori, Y. i. in *Modern aspects of electrochemistry* 89-189 (Springer, 2008).
- 42 Chernyshova, I. V., Somasundaran, P. & Ponnuram, S. On the origin of the elusive first intermediate of CO₂ electroreduction. *Proc. Natl. Acad. Sci.* **115**, E9261-E9270 (2018).
- 43 Hansen, H. A., Varley, J. B., Peterson, A. A. & Nørskov, J. K. Understanding Trends in the Electrocatalytic Activity of Metals and Enzymes for CO₂ Reduction to CO. *J. Phys. Chem. Lett.* **4**, 388-392 (2013).
- 44 Gattrell, M., Gupta, N. & Co, A. A review of the aqueous electrochemical reduction of CO₂ to hydrocarbons at copper. *J. Electroanal. Chem.* **594**, 1-19 (2006).
- 45 Gurudayal *et al.* Sequential cascade electrocatalytic conversion of carbon dioxide to C-C coupled products. *ACS Appl. Energy Mater.* **2**, 4551-4559 (2019).
- 46 Lum, Y. & Ager, J. W. Sequential catalysis controls selectivity in electrochemical CO₂ reduction on Cu. *Energy Environ. Sci.* **11**, 2935-2944 (2018).

- 47 Gao, J. *et al.* Selective C–C Coupling in Carbon Dioxide Electroreduction via Efficient Spillover of Intermediates As Supported by Operando Raman Spectroscopy. *J. Am. Chem. Soc.* **141**, 18704-18714 (2019).
- 48 Morales-Guio, C. G. *et al.* Improved CO₂ reduction activity towards C₂+ alcohols on a tandem gold on copper electrocatalyst. *Nat. Catal.* **1**, 764-771 (2018).
- 49 Vogt, H. On the supersaturation of gas in the concentration boundary layer of gas evolving electrodes. *Electrochim. Acta* **25**, 527-531 (1980).
- 50 German, S. R. *et al.* Electrochemistry of single nanobubbles. Estimating the critical size of bubble-forming nuclei for gas-evolving electrode reactions. *Faraday Discuss.* **193**, 223-240 (2016).
- 51 Zhao, X., Ren, H., Luo, L., Gas bubbles in electrochemical gas evolution reactions, *Langmuir* **35** 5392-5408 (2019).
- 52 Tan, Y. C., Lee, K. B., Song, H. & Oh, J. Modulating local CO₂ concentration as a general strategy for enhancing C–C coupling in CO₂ electroreduction. *Joule* **4**, 1104-1120 (2020).
- 53 Xu, W., Lu, Z., Sun, X., Jiang, L. & Duan, X. Superwetting electrodes for gas-involving electrocatalysis. *Acc. Chem. Res.* **51**, 1590-1598 (2018).
- 54 Wang, X. *et al.* Mechanistic reaction pathways of enhanced ethylene yields during electroreduction of CO₂–CO co-feeds on Cu and Cu-tandem electrocatalysts. *Nat. Nanotechnol.* **14**, 1063-1070 (2019).
- 55 Xing, Z., Hu, L., Ripatti, D. S., Hu, X. & Feng, X. Enhancing carbon dioxide gas-diffusion electrolysis by creating a hydrophobic catalyst microenvironment. *Nat. Comm.* **12**, 1-11 (2021).
- 56 Jung, H. *et al.* Electrochemical fragmentation of Cu₂O nanoparticles enhancing selective C–C coupling from CO₂ reduction reaction. *J. Am. Chem. Soc.* **141**, 4624-4633 (2019).
- 57 Loiudice, A. *et al.* Tailoring copper nanocrystals towards C₂ products in electrochemical CO₂ reduction. *Angew. Chem. Int. Ed.* **55**, 5789-5792 (2016).
- 58 Burdyny, T. *et al.* Nanomorphology-enhanced gas-evolution intensifies CO₂ reduction electrochemistry. *ACS Sustain. Chem. Eng.* **5**, 4031-4040 (2017).
- 59 Khan, S., Hwang, J., Horn, Y.-S. & Varanasi, K. K. Catalyst-proximal plastrons enhance activity and selectivity of carbon dioxide electroreduction. *Cell Rep. Phys. Sci.* **2**, 100318 (2021).
- 60 Yue, P. *et al.* Triple-phase electrocatalysis for the enhanced CO₂ reduction to HCOOH on a hydrophobic surface. *Chem. Eng. J.* **405**, 126975 (2021).

Acknowledgments

This work was supported by the Director, Office of Science, Office of Basic Energy Sciences, Chemical Sciences, Geosciences, & Biosciences Division, of the US Department of Energy under Contract DE-AC02-05CH11231, FWP CH030201 (Catalysis Research Program). ICP-OES was supported by the Microanalytical Facility, College of Chemistry, UC Berkeley. We thank College of Chemistry's NMR facility for resources provided and the staff for their assistance. Instruments in the CoC-NMR are supported in part by NIH S10OD024998. We thank Z. Zhou at the QB3 Chemistry Mass Spectrometry Facility for her assistance with GC-MS measurements. Computational work using COMSOL® Multiphysics was done at the Molecular Graphics and Computation Facility, UC Berkeley, which is supported by NIH S10OD023532. D.K. and S.Y. acknowledge support from the Samsung Scholarship.

Author contributions

S.L. and D.K. designed the experiments and analyzed data with assistance from Y.L. and M.G.; S.L. performed the experiments with assistance from D.K. and Y.L.; S.L. carried out the multiphysics simulation with assistance from D.K.; S.L. and M.G. designed and carried out the numerical model. P.Y. supervised the project and experimental design. All authors wrote the manuscript.

Competing interests

Authors declare no competing interests.